ADVANCED INTELLIGENT SYSTEMS
Open Access
www.advintellsyst.com

Bioinspired Moisture-Driven Soft Robotic Actuator

*Akshay Balachandran, Nair Abhigith Ravindran, Ghulam Mohd, Irfan Majeed Bhat, Saswati Priyadarshini, and Saifullah Lone**

Multifunctional materials in nature, utilizing atmospheric water content, offer solutions to challenges in soft-actuating materials research. The leaf of *Arundo donax*, an invasive plant, showcases exceptional properties: structural integrity, passive actuation, tunability, load-bearing capacity, longevity, and an integrated battery-free fluid generation and distribution mechanism. These functions coexist within a thin (≈130 μm) and lightweight structure with simple compositions. The study investigates material composition, passive fluid transport, water harvesting structures, and mechanical properties, revealing unexpected correlations between surface and internal structures. Additionally, tunable actuation, suitable for origami-based mechanisms, is explored. Testing an energy-free, moisture-triggered soft robotic gripper, its ability to lift over 50 times its weight while maintaining sufficient softness for delicate tasks is demonstrated. This unit-wise structure-based actuation offers promise for soft robotics, with favorable fabrication possibilities and motion manipulation.

1. Introduction

The need to create actuator materials that are soft enough to perform delicate and intricate actions seemingly impossible for conventional stiff and rigid materials increased as the field of robotics developed over the last four decades. Even though significant development happened in solving the challenges in this field, some issues persist. Widely used soft actuator materials use pneumatic actuation or fluid-induced shape-changing mechanisms. Bulk fluid pumping systems with heavy batteries restrict the use of these actuator systems in many functional applications.[1] By introducing water-absorbing and swelling materials, this problem is solved to an extent.[2] Jia-Nan et al. engineered an asymmetric structure of quantum-confined superfluid (QSF) on both sides of the MXene film, resulting in nonuniform adsorption, transportation, and desorption of water molecules within the QSF network. This configuration led to improved actuation performance.[3] Yu-Qing et al. provided examples of various bioinspired actuators utilizing the moisture-responsive properties of graphene oxide (GO). The ultrafast permeation of water through a GO membrane enables highly sensitive and smooth actuation.[4] Similarly, multiple material systems are used as an alternative to the energy expensive systems.[5–7] Nonetheless, the problem of reliability, load-bearing capacity, controllability, and fabrication made it challenging to apply these materials directly to real-world applications.[8]

The nonlinear arrangement of materials in natural actuators recently got attention because these materials with simple components of swelling and stiff parts achieve highly efficient passive actuation mechanisms. Passive plant actuation, typically observed and widely studied in various species, consists of a complex distribution of plant materials like lignin and cellulose microfibrils, enabling undesired differential swelling or shrinkage leading to actuation.[9–16] Based on the arrangement of hygroscopic swelling materials and cellular structure, plant parts exhibit different passive movements like bending,[11] curling,[9] twisting,[17] and coiling.[14] Generally, continuous gradient arrangement of lignified and nonlignified cells creates uneven water absorption and swelling mechanisms. For example, the hydroresponsive bending of dandelion pappus hair is due to the radial arrangement of at least four different tissue types with strongly lignified vascular tissue and hydrophilic apical plate side cell arrangement in a bilayer fashion.[10] Hydration-induced actuating structures like resurrection plant,[9] dandelion pappus,[10] pine cone,[11] ice plant seed capsule,[12] wheat awns,[13] and stork's bill awn[14] are studied and put forward as a promising biomimetic model in fields like soft robotics. However, most of these biomodels are complex and only intended to perform a specific action, hence lacking adaptive flexibility.

A. Balachandran, G. Mohd, I. M. Bhat, S. Priyadarshini, S. Lone
Department of Chemistry
National Institute of Technology (NIT)
Srinagar, Jammu and Kashmir 190006, India
E-mail: saif.lone@northumbria.ac.uk

A. Balachandran, N. A. Ravindran, G. Mohd, I. M. Bhat, S. Priyadarshini, S. Lone
iDREAM (Interdisciplinary Division for Renewable Energy & Advanced Materials)
Laboratory for Bioinspired Research on Advanced Interface and Nanomaterials (BRAINS)
NIT
Srinagar, Jammu and Kashmir 190006, India

S. Lone
Department of Physics, Faculty of Engineering and Enviornment
Northumbria University
Newcastle upon Tyne, North East NE77YT, United Kingdom

The ORCID identification number(s) for the author(s) of this article can be found under https://doi.org/10.1002/aisy.202400609.

© 2024 The Author(s). Advanced Intelligent Systems published by Wiley-VCH GmbH. This is an open access article under the terms of the Creative Commons Attribution License, which permits use, distribution and reproduction in any medium, provided the original work is properly cited.

DOI: 10.1002/aisy.202400609

Here, we observed a profound correlation between material composition, mechanical arrangement, passive fluidic motion, and atmospheric water harvesting structures, enabling multifunctional and controllable actuation mechanisms. This fascinating hinged single-unit actuation system is observed in invasive *Arundo donax* species.[18] Different strategies are adopted among plant species to survive low water availability. Two of the most common strategies are reducing plant and leaf surface area to prevent evaporation[9] and atmospheric water harvesting.[19] We found out that *A. donax* used both strategies to spread over large areas of land successfully. Further studies revealed much more exciting aspects of the interconnected curling and water harvesting mechanism strategy. To prevent water loss and long-term survival, leaves and stems of some plant species tend to curl upon dehydration and return to normal on rehydration. The best-known example of this kind of curling mechanism is observed in the resurrection plant or *Selaginella lepidophylla*. The stem is curled from top to bottom in varying degrees due to a nonuniform or gradient arrangement of hydrophilic and hydrophobic materials.[9] In the *A. donax* plant, while leaf curls, the mechanism to harvest water and retain its initial shape is enhanced.

Meanwhile, a simple repetitive unit actuation system model of this plant material can be fabricated easily using techniques like 3D printing artificially. Such a model can fabricate continuous sheets of actuators with controlled movement direction even after fabrication. As *A. donax* is a commonly observed invasive species that can grow into a massive vegetation group,[20,21] its phytochemicals,[22,23] material aspects,[24–26] and plant structure[27] are widely studied. Even though it displays dramatic thermotropism to prevent water loss, there are no significant studies conducted on its leaf-curling mechanism. The leaf of a giant reed is thin (≈120–150 μm) and segmented by longitudinal veins running parallel to the leaf's midrib. As this plant species is one of the fastest-growing grass species with little nutrients, water transport throughout these thin leaf layers is very efficient.[27,28] The hydrophobic top and bottom leaf surfaces bind this efficient water transport system through hydrophobic and hydrophilic parts. This and the possible combination of moisture-sensitive actuation and curling angle control make this plant actuator model unique from previous ones.

2. Results and Discussion

2.1. Efficient and Restricted Fluid Pathways for Hydroresponsive Actuation

A. donax leaf curls (**Figure 1**) upon losing water from the leaf body. When rehydrated, the leaf will uncurl and return to its original position. This cycle can be repeated more than 50 times.

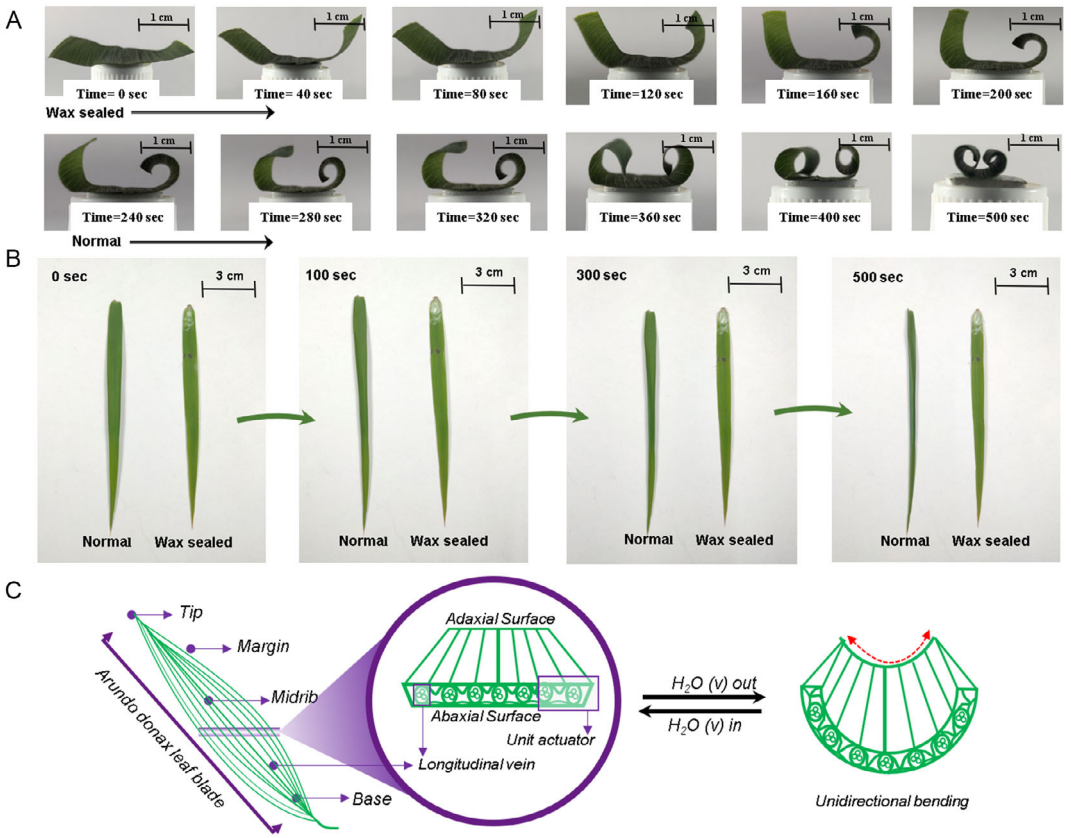


Figure 1. Controlled passive fluidic motion-assisted actuation in *A. donax*. A,B) Central capillary network blocking experiment. The comparative actuation of paraffin wax blocked central capillary network (CCN) and nonblocked CCN in (A) leaf segments and (B) entire leaves. C) Schematic diagram explaining the general plant morphology and its relationship with actuation mechanism; leaf curls only toward the adaxial surface along the midrib.

© 2024 The Author(s). Advanced Intelligent Systems published by Wiley-VCH GmbH

This relatively quick response to hydration and dehydration is because of the efficient network of central microcapillary tubes (CMT) running between the leaf's hydrophobic top and bottom layers. The veins of leaf blades run from the leaf base to the leaf tip like a longitudinal parallel vein (LPV) arrangement, dividing the leaf into parallel segments as schematically shown in Figure 1C. The vascular system runs along these LPVs and is confined between the top and bottom surface layers.[21,27,28] This CMT is made up of variously sized vascular bundles. These vascular bundles are made up of vascular tissues called phloem and xylem. These are further enclosed with two layers of bundle sheath cells: outer thin-walled and inner thick-walled bundle sheath cells.[21] The leaf curls toward the upper surface in a vector perpendicular to the LPV. To test the closed pathway for hydration and dehydration, we sealed the base consisting of capillary tubes of an entire leaf with paraffin wax and compared its actuation with a nonsealed whole leaf side by side (Figure 1B). The leaf with a wax-sealed base part nearly stopped its actuating mechanism, while the typical leaf curled completely. This proved the strict involvement of CMT in transporting water for both hydration and dehydration, aiding the actuation mechanism. Transpiration and other types of water loss do not directly affect actuation. This is further proved by comparing the actuation speed of the leaf segment of length 1 cm dissected perpendicular to the LPV of the leaf. By comparing the degree of actuation after 10 min, both wax-sealed samples did not curl. The dissected small piece of leaf curled faster to a greater degree of curling than the entire leaf blade (Figure 1A). This is because of the increased water transport of the segment due to the small distance and exposed ends. Further, this length to curling speed is studied by testing the degree of curling concerning the length of the leaf segment in a fixed temperature and humidity. It showed the expected increase in curling speed upon a decrease in leaf segment length (Figure S2a, Supporting Information). Another factor influencing the rate of capillary evaporation is the temperature. A test done with the degree of curling concerning varying temperatures in a fixed humidity and dimension of leaf segment proved that the speed of curling depends on an increased rate of evaporation at high temperatures (Figure S2b, Supporting Information).

The efficiency of passive fluid transportation via microsized capillary tubes is primarily due to a confluence of factors. First off, a major factor in this phenomenon is the capillary tubes' irregular and tapered diameter and shape. Research, like that of Jean et al. has highlighted the advantage of capillary rise that tapered tubes have over those with constant radii, as explained by the Washburn law.[29] Furthermore, by allowing fluid to flow through connected channels, the tubular network structure that these systems are built with enhances their efficiency even more. Furthermore, the micro roughness of the capillary tube inner walls is crucial. With its uneven surface characteristics, this roughness helps to lower the contact angle, which raises capillary rise in the microchannel network.[30] From these experiments, we concluded that the actuation speed primarily depends on the water flow rate through the CMT. According to the Hagen–Poiseuille equation,[31] the flow rate of fluids through the straight, smooth microcapillary tubes is given as

$$q = \frac{\pi d^4 \Delta P}{128 \mu L_o} \tag{1}$$

Here, μ is the fluid viscosity, d is the capillary diameter, and ΔP is the pressure drop along the capillary and can be calculated by Equation (2):

$$\Delta P = \frac{2\sigma \cos\theta}{r L_o} \tag{2}$$

where L_o is the length of the capillary tube, θ is the contact angle between water and the capillary wall in degrees, r is the radius of the capillary tube, and σ is the surface tension of water. The average diameter of the CMT observed in the leaf sample through field emission electron scanning microscopy (FESEM) characterization is 8–12 μm (**Figure 2**A,B). Ideally, the flow rate in these CMTs must be low, as the flow rate, according to Equation (1), is directly proportional to the fourth power of tube diameter. However, the experimental observations at room temperature and atmospheric pressure with 70% humidity show the starting of actuation right after 1 s for a sample of 3 cm in length (Figure 1D and S1, Supporting Information). This efficiency in passive fluid transportation using microsized capillary tubes is mainly because of the tapered and irregular capillary tube diameter and shape, tubular network structure, and capillary wall microroughness (Figure S4, Supporting Information).

2.2. Repeating Thin Bilayer Unit Actuation Drives Directional Curling

The involvement of CMT in efficient hydration and dehydration mechanism in the leaf blade is tested and proved. We observed the absorption of these transported water into certain specific regions in a bilayer repeated fashion throughout the leaf blade, enabling actuation. Surprisingly, the shrinking and expanding parts that make the leaf curl inward are arranged on both sides of LPV (Figure 1 and 2A,B). These two shrinking and expanding parts placed on both sides of LPV constitute the top layer hinge (TLH) of our unit bilayer actuator (UBA). The base part of our UBA consists of a layer below the LPV with mild shrinkage and expansion properties.

We found the entire leaf curls due to the repeating UBA structure arranged like a little hinged unit along the LPV. Each LPV acts as a longitudinal hinge that can only be turned upward (Figure 1C,D and Movie S3, S4, Supporting Information). This enables the entire length of the leaf to curl and close the upper surface entirely. When we examine the leaf strip dissected by cutting along the line perpendicular to the LPV, the involvement of UBA becomes clearer.

Several external factors like temperature, UBA length, maturity of the leaf, flexibility, and arrangement of the UBA influence this unit bilayer actuation. A comparative experiment on the influence of temperature on the actuation proved that the increase in temperature increases the actuation speed due to an increased dehydration rate (Figure S2b, Supporting Information). The plant actuation specimen can withstand up to 80 °C, and beyond that, the performance decreases due to the thermal structural destruction. Thermogravimetric analysis and derivative thermogravimetry (TGA DTG) of the plant

© 2024 The Author(s). Advanced Intelligent Systems published by Wiley-VCH GmbH

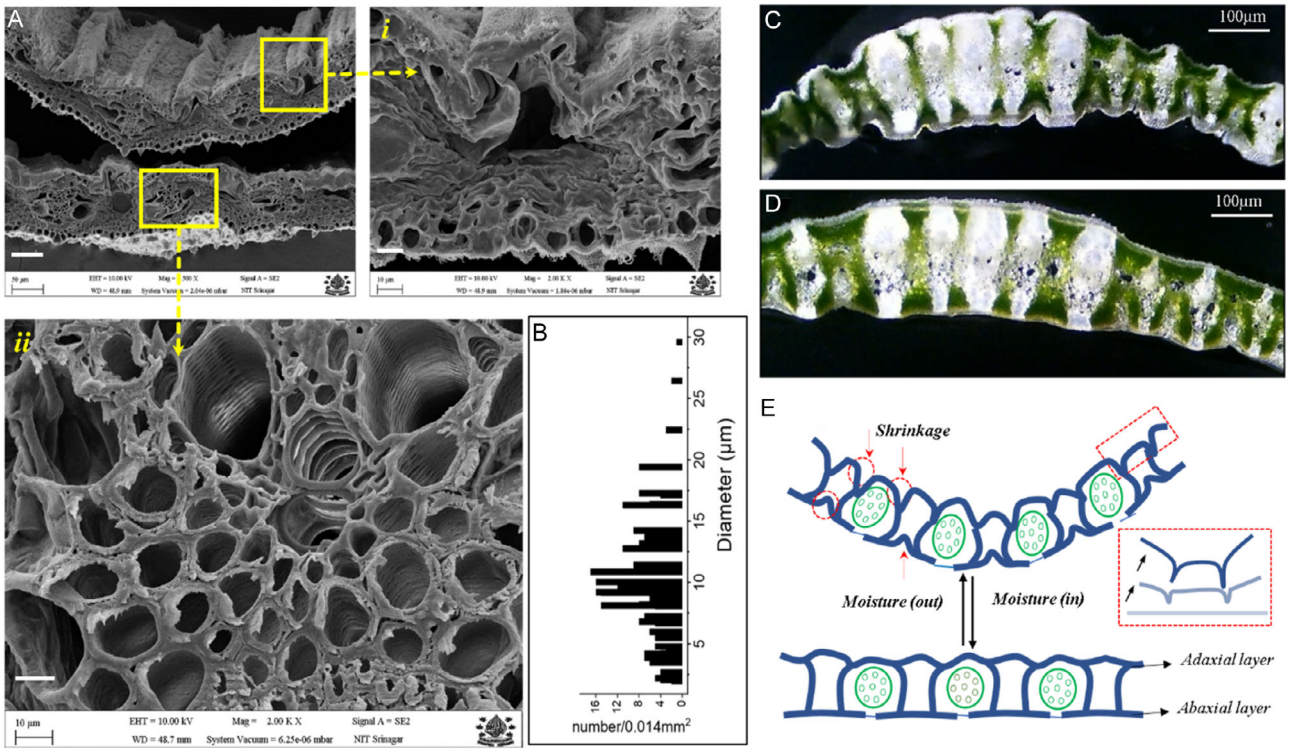


Figure 2. Physical features of capillary and unit shrinkage system. A) SEM images of the actuated cross section of leaf dissected perpendicular to the longitudinal vein: i) shrinkage of the actuating structures on both sides of the longitudinal vein; ii) central capillary tubes. B) Distribution of capillary tubes with respect to diameter. C,D) Optical microscopic image showing (C) dehydrated leaf cross section and (D) hydrated leaf cross section. E) Schematic showing unit shrinkage mechanism with actuating microstructures.

samples showed the complete loss of absorbed water at ≈90 °C and beyond 300 °C, full material breakdown (**Figure 3**C).

The length of the UBA also influences the actuation speed. The test uses various sized leaf segments or UBA with increasing length. It clearly showed that the actuation speed increases with increased actuator size (Figure S2a, Supporting Information). This is primarily because of the decrease in flexibility as the length of UBA increases and because of the increase in load contributed by the increased length of the sample. This is proved by testing young and mature leaves side by side (Figure S2, Supporting Information). Young leaf material exhibits superior flexibility because the lignified tissues are not fully grown. Young leaf segments are also relatively lightweight, and thus, they curl faster than matured ones. This was again tested with temperature-dependent curling, too. Young leaf segments showed faster actuation in both cases than matured leaf segments. As the TLH is arranged along with the LPV, and each longitudinal unit will actuate precisely in the direction vector perpendicular to the LPV, the arrangement of longitudinal UBA in each segment will determine the nature of actuation. We will discuss this in detail later in this article.

Detailed UBA analysis sheds light on the actuation mechanism's essential yet relatively simple geometrical and material aspects. By observing the real-time actuation mechanism through an optical microscope (Figure 2C,D), we identified that the UBA comprises three unique shrinking structures and three other stiff supporting structures. This simplified model is further proved by FESEM images (Figure 2A) of the cross section of the leaf blade dissected perpendicular to the LPV (transverse section of the leaf blade). The SEM images of the curled samples displayed shrunk microstructures in the UBA. During the curling mechanism (Figure 2E), the two strips of microactuators will curl inward, leaving the central longitudinal strip intact. At the same time, a minor microactuator at the bottom of the stiff structure will also bend relatively less inward. This causes uneven shrinkage in the bilayer overall structure of the leaf material. The bilayer fashion of material arrangement is identified using Energy-dispersive X-ray analysis (EDAX) analysis (Figure 3D and S7, Supporting Information). The LPVs and the central support will remain stiff and support the actuation mechanism.

The transverse section of the leaf blades stained with fuchsin dye revealed the arrangement of the hydroresponsive and stiff lignified part of the UBA (Figure 3A,B). The lignified part, visible as a bright red coloration, holds the structure in three distinct parts: one in the middle of the two adaxial microactuators and two on both sides of the adaxial and abaxial microactuators. Strong peaks around 1500 cm^{-1} in Raman spectra (Figure 3E) indicate the presence of lignin, and peaks at 1600 cm^{-1} indicate the presence of phenolic compounds.[1] The presence of interconnected lignin and hemicellulose is detected by Fourier transform infrared spectroscopy (FTIR) peaks (Figure 3F) at 1600 cm^{-1} due to –COO– stretching in hemicellulose and aromatic skeletal stretching. Further peak at 1734 cm^{-1} indicates the presence of C=O conjugates in hemicellulose.

© 2024 The Author(s). Advanced Intelligent Systems published by Wiley-VCH GmbH

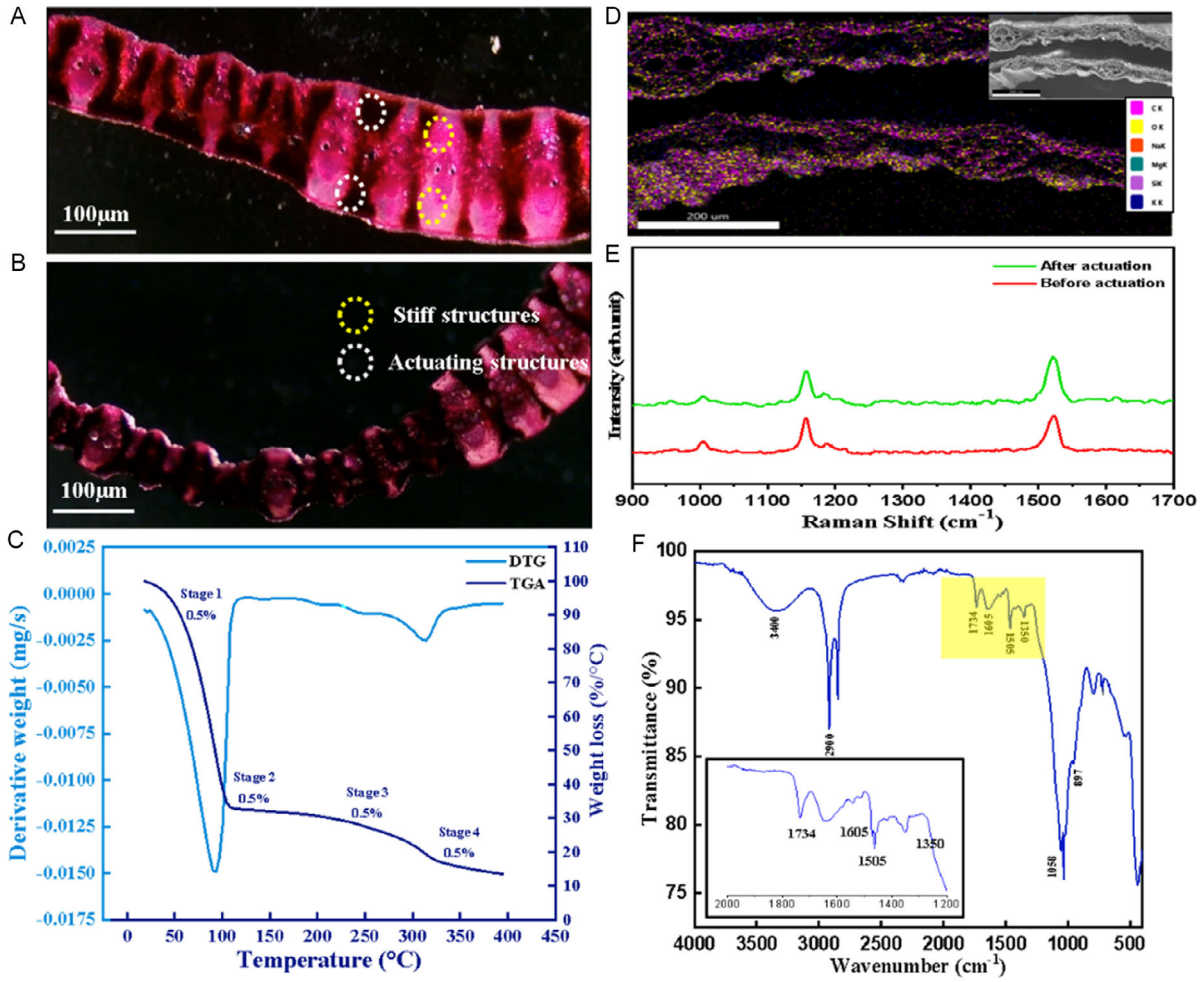


Figure 3. Chemical composition driving actuation mechanism. A,B) Optical microscopic image showing a cross-sectioned sample dyed with fuchsin, bright red parts of stiff nonactuating lignin material, and dark parts of hydrophilic actuating parts: before actuation (A) and after actuation (B). C) TGA DTG analysis showing significant mass loss in stage 2 due to water evaporation and final degradation at stage 4. D) EDAX data showing the distribution of elements in the leaf cross section revealing bilayer structure; SEM image is given inset. E) Raman spectroscopic data taken before and after losing water content leads to actuation. F) FTIR data revealing interconnected lignin–cellulose–hemicellulose polymers.

Interconnected arrangement of lignified and nonlignified parts, thus causing nonuniform swelling and actuation in the material. Bulliform or motor cells are found in the microactuating parts on the adaxial surfaces. Bulliform cells are hollow cells enabling hinge-like mechanism, and these are larger and found to be extended into the mesophyll area, allowing efficient actuation.[32]

2.3. Surface Microthorn Induced Moisture Capturing and Actuation

The adaxial and abaxial surface of the leaf exhibits different properties. As the leaf actuates toward the adaxial surface, the surface consists of more distinguished longitudinal strips that act like hinges during actuation (**Figure 4**A,B and S6b, Supporting Information). The abaxial surface has a droplet-pinning effect (Figure S3, Movie S2, Supporting Information). It is more hydrophobic, with an average contact angle of 138° than the adaxial surface, with an average contact angle of 136° (Figure 4A,C). Micro/nanostructures on the surfaces of the leaf are the reason for the hydrophobic properties. The humidity chamber experiments revealed the atmospheric water harvesting capability of leaf surfaces. The surface structures must have the structural features for droplet formation and transportation for efficient and fast atmospheric water harvesting. We observed the formation and transportation of water droplets on the leaf's surface using an optical microscope (**Figure 5**B and Movie S5, Supporting Information). Droplet formation and transportation are observed to be faster on the abaxial surface. Further examination of both the abaxial and adaxial leaf surface of the leaf using FESEM revealed microsized conical structures with an approximate height of 4–7 μm (Figure 4D, 5D–F and S6a,c, Supporting Information), with an ideal shape suitable for atmospheric water harvesting.[19] Although microhair-like structures seen on both leaf surfaces also aid in atmospheric water harvesting (Movie S6, Supporting Information), the main contribution is from surface microthorn (SMT) structures.

© 2024 The Author(s). Advanced Intelligent Systems published by Wiley-VCH GmbH

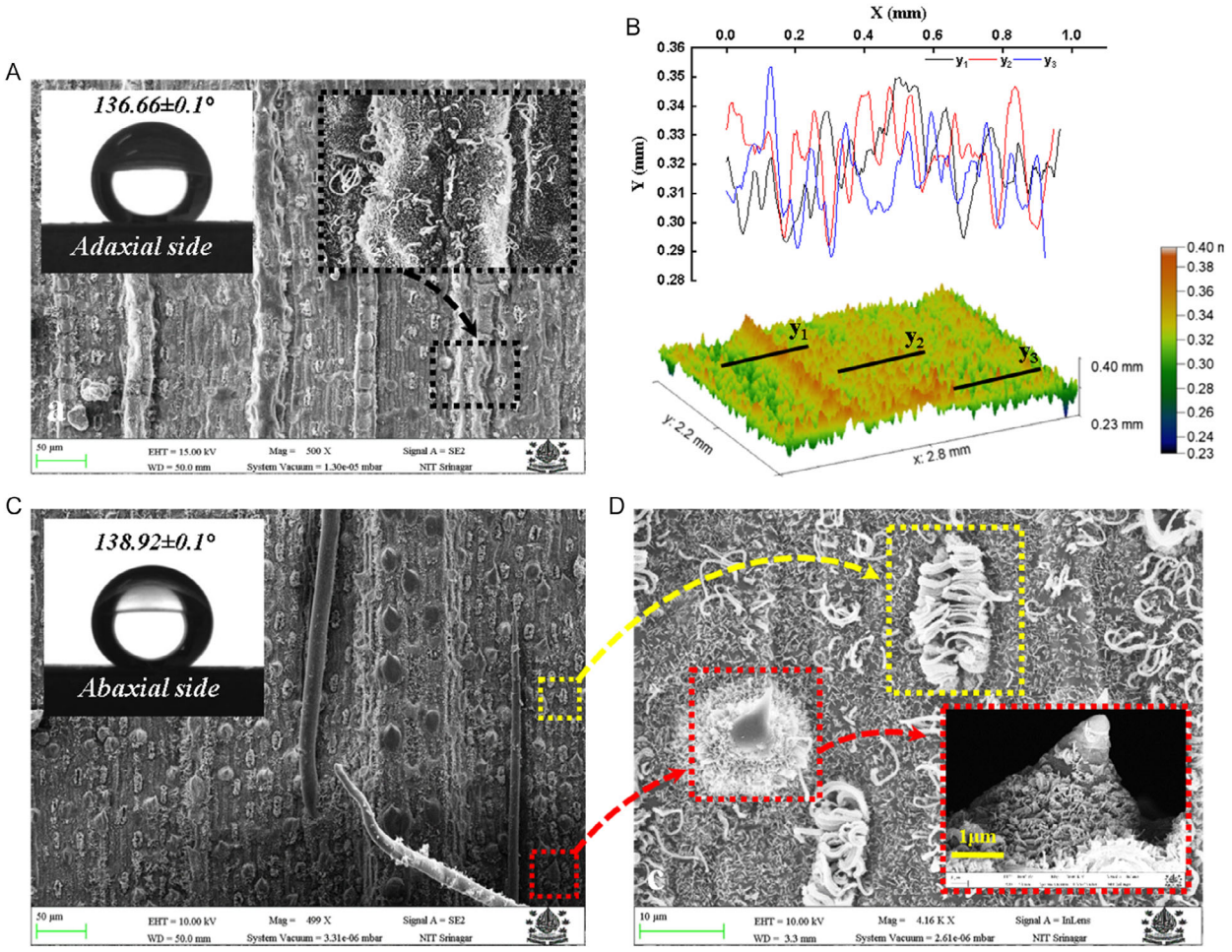


Figure 4. Adaxial and abaxial surface features of *A. donax* leaf. A) SEM image of the adaxial surface with zoom-in image of LPV part showing microfibers. Contact angle data are given inset. B) 3D profilometer images of the leaf's adaxial surface show frequent surface projections. C) SEM image of abaxial side with static water contact angle given in inset. D) SEM images showing conical structures in the abaxial side.

Conical structures with variable wettability are the most efficient for capturing water from the atmosphere because the Laplace pressure gradient, gravitational force, and surface energy gradient can simultaneously influence droplet formation and transport. SMT has an overall unique structure that can efficiently aid the formation of water droplets from atmospheric moisture and the quick transportation of droplets to the leaf surface. SMT can be divided into three parts: tip section, midsection, and base part, as shown in Figure 5C. The tip part of the SMT is a hydrophilic spot and works as the active spot for droplet nucleation and growth. It is observed that water droplet is formed and enlarged to optimum size at this tip spot and then immediately released toward the base part. The tip angle β is below 20°, and it is observed that a lower conical tip angle is favorable for faster droplet transport and, hence, a high rate of water harvesting.[33] The top tip surface of the SMT does not seem to have hydrophobicity-inducing micro/nanostructures. This explains rapid microdroplet formation and immediate transportation on the leaf's surface.

The midsection of the SMT contains a gradient arrangement of nano/microsurface structures and thus exhibits variable wettability. This creates a surface energy gradient that drives water droplets formed on the tip toward the base. The driving force[34] created by this surface wettability gradient is given as Equation (3):

$$F = \int_{l_{tip}}^{l_{base}} (\mathrm{Cos}\theta_1 - \mathrm{Cos}\theta_2)\mathrm{d}l \tag{3}$$

Here, θ_1 and θ_2 are the advancing and receding contact angle of the middle section, and dl is the integral variable along the length of the middle section from the region near the tip (l_{tip}) to the region near the base (l_{base}). Additionally, this curved conical structure[35–37] contributes to forming the Laplace pressure gradient given by the Equation (4):

$$\Delta P = \frac{2\gamma}{(r+n)} \tag{4}$$

Here, r is the radius of curvature, γ is the energy, and n is the height of the droplet from the cone axis ($D/2$). The base part of

© 2024 The Author(s). Advanced Intelligent Systems published by Wiley-VCH GmbH

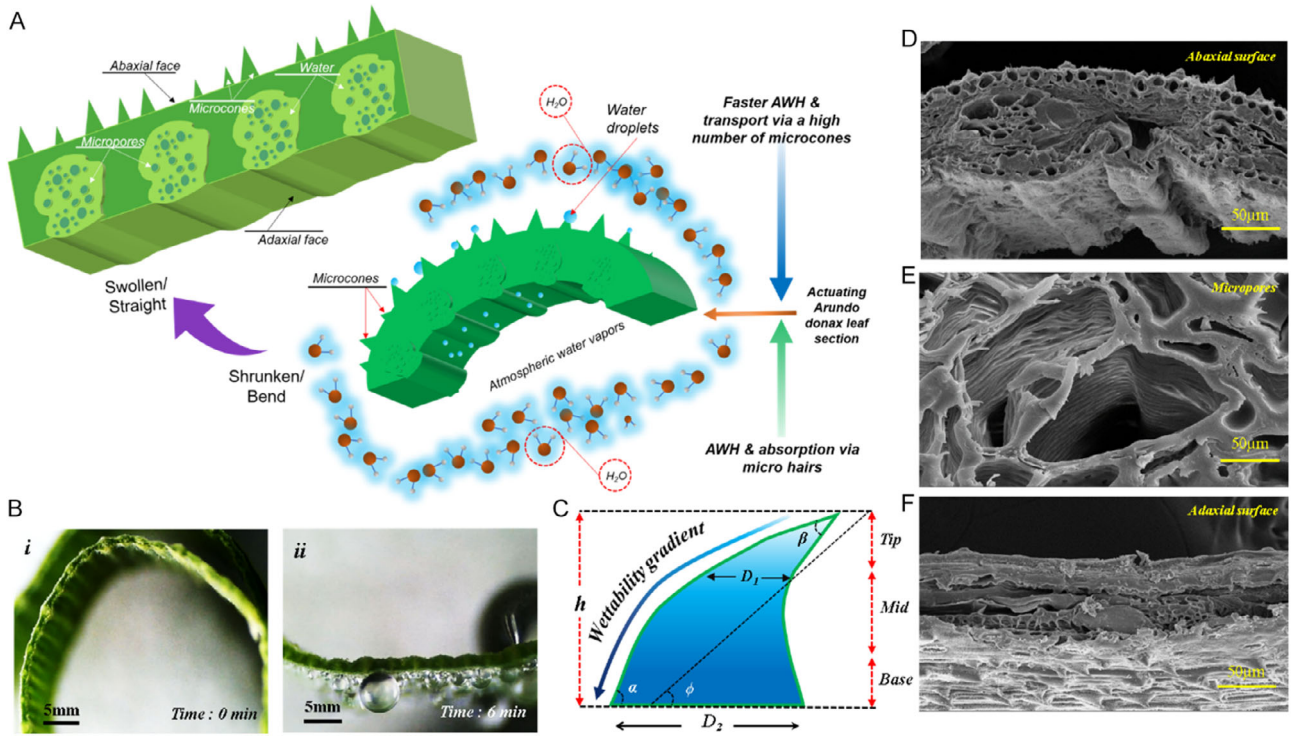


Figure 5. Interconnection between atmospheric water harvesting and actuation mechanism. A) Schematic representation of moisture sensitive actuation mechanism, i.e., atmospheric water content harvested by surface structures is absorbed by hygroscopic part to facilitate actuation mechanism. B) Optical microscopic images of leaf material: i) curled state in an atmosphere with 95% humidity and 13 °C temperature; ii) sample uncurled after 6 min with harvested water droplets on its surface (scalebar 0.5mm both). C) Structural analysis of microthorn. D) SEM image showing a cross section of *A. donax* leaf with microthorn structures in the abaxial surface. E) SEM image showing a cross section of *A. donax* leaf with micropores. F) SEM image showing a cross section of *A. donax* leaf with adaxial surface.

the cone contributes to the Laplace pressure gradient with a larger diameter and base angle α. A cone with a micrometer ranged height (h) will exhibit faster droplet transportation with a long base diameter and proportionally less base angle aiding the curvature.

As most SMTs are seen on the abaxial surface, the structural features enabling high surface energy gradient and Laplace pressure gradient significantly contribute to the water harvesting and movement against the gravitational force. This abaxial water harvesting effect is observed in other species too[38] but what makes things interesting is that during the actual occasion when water harvesting is necessary for actuation, gravitational force will also aid the transportation of droplets and hence speed up the process even further—the leaf curls toward the adaxial surface during low atmospheric moisture content or water availability. As the leaf begins to actuate, the SMT orientation will change from tip facing down to tip facing upside (Figure 5A,B,D). This will induce gravitational assistance in water harvesting and actuation. The SMT inclination angle ϕ makes it easier to achieve gravitational assistance for droplet transport. This is a brilliant survival adaptation mechanism of this plant species because when more water is needed for the plant, the leaf curling upward will not only stop the transpiration loss from the upper surface but also initiate high-speed atmospheric water harvesting and transportation mechanism of the bottom surface. This interrelation between atmospheric water harvesting and the actuation mechanism is tested multiple times. It is also proved that such interconnected mechanisms can be used in battery-less actuation systems.

2.4. Force and Bending Per Unit Actuator: Characteristics and Potential Applications

We conducted a series of strength and functional tests by taking a leaf sample dissected perpendicular to LPV. The sample is 3 cm long perpendicular to LPV and is 1 cm in breadth (LPV length). The material has a thickness of ≈130 μm. The weight of the sample varies with the maturity and nature of the leaf sample taken, but on average, the weight of the sample is in the range of 0.03–0.085 gm. Despite the material sample's fragile and lightweight nature, it exhibited remarkable mechanical properties, showing a range of functional applications.

Weight loss is measured with the degree of actuation to determine the relation between water evaporation and actuation (**Figure 6**B). For each 360° curling actuation, an average of 12% of the sample weight is decreasing. Even though the degree of curling (λ) is inversely proportional to the mass of water evaporated (m), a material constant also influences the relation. Avoiding all external factors in the actuation mechanism other than the hydration and dehydration mechanism, the material constant

© 2024 The Author(s). Advanced Intelligent Systems published by Wiley-VCH GmbH

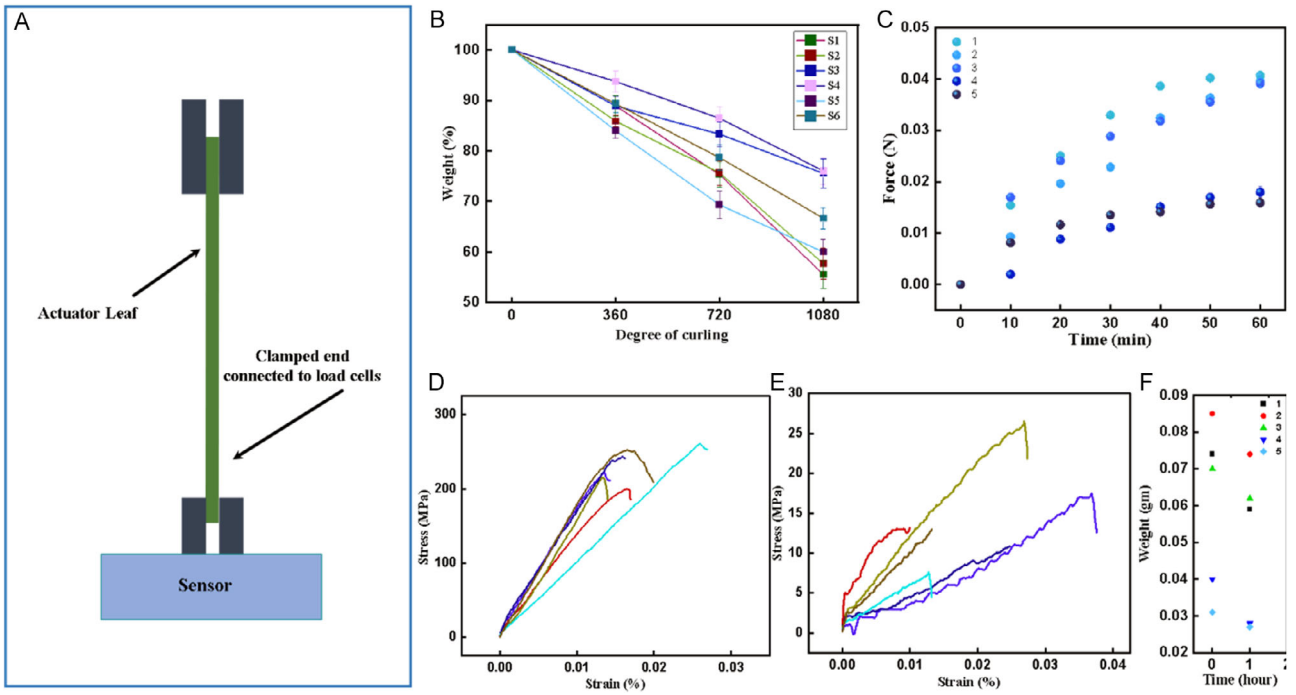


Figure 6. Mechanical Strength and load-bearing capacity of the actuator leaf material. A–C) The experiment was conducted to test the force generated by the actuation mechanism of the leaf materials with a length of 3 cm and breadth (along longitudinal vein) of 1 cm at a temperature of 10 °C and humidity of 70%. Five-leaf sections are tested from the leaf's base to the tip (1–5). (A) Schematic representation of setup designed to measure the force generated by curling of the leaf material. (B) Relation between degree of curling and weight loss due to evaporation; six-leaf sections are represented (starting from base S_1 to S_6). (C) Graph showing the relation between Force generated with respect to time during curling force test. D) Stress–strain graph of leaf section with 3 cm length (along the vein) and 1 cm breadth. E) Stress–strain graph of leaf section with 3 cm length and 1 cm (along the vein) breadth. F) Weight loss of the samples after the curling force test.

that significantly affects the degree of actuation is stiffness factor (s). The bilayer material composition must have the highest possible flexibility for smooth actuation. Cell walls become relatively highly lignified for mature leaves and the stiffness factor increases. This is not the case for young leaves; thus, young leaves can actuate faster than mature ones. This is observed in a series of experiments conducted on different leaf samples.

Further, to test the influence of stiffness factor in different plant materials, samples are placed between two smooth surfaces and crushed under 5 kg of weight (Figure S8, Supporting Information). Crushed samples exhibited faster actuation than normal ones because the stiffness factor was changed. Thus, the degree of curling can be related to the mass of the water evaporated with the Equation (5):

$$\lambda = \frac{s}{m} \tag{5}$$

Evaporative water loss causes the leaf material to undergo a curling actuation mechanism. Even though the mechanism enables the leaf curling, it exhibited remarkable force that allows the material to lift weights more than 50 times the weight of the sample (**Figure 7**B). To measure the average force generated with time during the dehydration actuation mechanism, we used a setup in which the sample is clamped between a fixture and a load cell (Figure 6A). When the material begins to actuate, the load cell records the force generated. We studied the force generated every 10–60 min at a temperature of 10 °C, atmospheric pressure, and humidity of 50% (Figure 6C,F). A linear relation is observed due to the constant shrinking rate with water loss due to fixed experimental conditions. After 30 min, the linearity began to be disrupted because the lift capacity of actuation began to decrease. After 60 min, the actuation seems to be stopped because the opposing force nearly equaled the force exerted by the actuating material. For every test, sections from different parts of the leaf are taken; therefore, the force exerted becomes different for the same conditions. The leaf's base and middle parts exhibited higher force than the tip sections. This is because of the in-between distance and thickness of the LPV and interconnecting actuating structures. Before starting the testing at time 0 and after 60 min, the mass of the samples used for testing is measured, and it found that, on average, 12% of the weight is lost. This corresponds to a 360° curling limit according to the weight loss experiment.

Load-bearing capacity is tested using samples dissected perpendicular and parallel to LPV (Figure 6D,E). Samples dissected parallel to LPV (LPV length 3 cm) can bear loads of more than 40 N before material failure. This is because of the solid and stiff fibrous network along the LPV that acts as a skeletal structure. On the other hand, samples dissected perpendicular to LPV (LPV length 1 cm and sample length 3 cm) have shown significantly lower load-bearing capacity. This is because of the lack of LPV skeletal support along the vector line of force. LPV lies

© 2024 The Author(s). Advanced Intelligent Systems published by Wiley-VCH GmbH

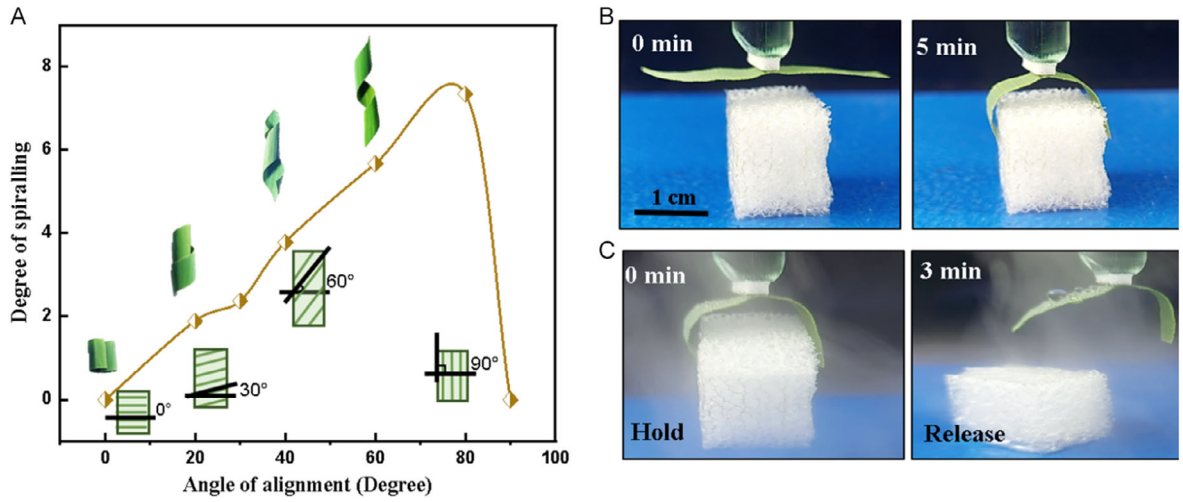


Figure 7. Functional applications. A) Relation between longitudinal vein alignment angle and extent of spiraling actuation. B,C) Moisture-controlled soft robotic gripper model from *A. donax* leaf. (B) Low moisture atmosphere triggering downward actuation and material holding. (C) A high moisture atmosphere triggers the release of held material by opposite actuation direction.

perpendicular to the force direction and in between space consists of soft actuating materials with less load-bearing capacity. This material thus exhibits directional load-bearing capacity due to the unique arrangement of stiff and actuating materials.

The unit-wise hinged actuation mechanism also provides a unique ability to control spiraling actuation concerning the angle of LPV arrangement. During most of the actuation experiments conducted in this study, the material segments from leaf samples are taken by dissecting the leaf perpendicular to the LPV (the dissection line and LPV line have a 90° angle). This always leads to perfect curling of the sample during actuation, or the distance between two ends is always the same during actuation. But as the angle of alignment changes, this distance changes (degree of spiraling). The degree of spiraling increases between 0° and 90° angle of alignment (Figure 7A). This is a perfect example of simple, tuneable actuator material. This property is ideal for origami-type self-organizing materials. Using this material, we also demonstrated the possibility of a battery-less moisture-triggered soft robotic gripper model (Figure 7B,C and Movie S7, Supporting Information). The material can pick and place soft materials in response to atmospheric moisture. This thin gripper can even hold water droplets (Movie S8, Supporting Information), opening many possibilities.

3. Conclusion

There are vast data of unveiled structural and compositional properties of natural materials enabling complex, efficient multifunctional properties like actuation mechanism. Even though advanced fabrication techniques like additive manufacturing are expanding rapidly, the complex structural and compositional properties of reported natural material structures enabling functions like actuation are challenging to mimic. Here, we report a relatively simple natural material model with two interconnected functionalities that can be emulated using present-day fabrication methods. It is often fascinating how plants develop diverse survival properties. Most of the time, those are the best lessons for material scientists. One example is interconnected leaf actuation and water collection from moisture exhibited by the *A. donax* plant species. The plant material's unique structural and compositional properties enable efficient fluid transport, water collection from moisture, directional mechanical properties, and controlled unit actuation mechanisms. Comparatively fast fluid transport in the microcapillary tubes is primarily because of the rough capillary walls, branched structure, and nonuniform capillary diameter. Actuation is enabled by a simple bilayer unit actuator structure consisting of microactuating units with cellulose, hemicellulose, and lignin networks arranged suitably.

A fascinating mechanism observed is the connection between this actuation and the water-harvesting mechanism of surface structures. A detailed study of the adaxial and abaxial surface of the plant revealed that even though both surfaces are hydrophobic, the abaxial surface has a pinning effect and consists of many conical structures compared to the adaxial surface. This gives the abaxial surface harvest water from atmospheric moisture, even against gravity. When water is lost, the leaves curl upward to prevent water loss from the adaxial surface. Due to this curling, the conical structures in the abaxial surface began to slowly align upward and get gravity assistance in water harvesting, speeding up the process. This enables the decurling process due to the supply of harvested water to the plant. The directional curling and mechanical properties make this material a perfect model for various multifunctional materials with applications in soft robotics, actuators, self-assembling materials, water harvesting structures. We hope this material model can bring a revolutionary change in the concept of simple interconnected mechanisms in material design.

4. Experimental Section

A detailed explanation of materials and methods and Figure from S1 to S8 are given in Supporting Information. Movies S2–S8, Supporting Information are also provided.

© 2024 The Author(s). Advanced Intelligent Systems published by Wiley-VCH GmbH

Supporting Information

Supporting Information is available from the Wiley Online Library or from the author.

Acknowledgements

This work was supported by SERB (Science & Technology Research Board)—a statutory body under the Department of Science & Technology, Government of India, under the Research grant of the Ramanujan Fellow Award (File number: SB/S2/RJN-013/2018). Also, this work was partly funded by Northumbria University, Newcastle, upon Tyne NE7 7XA, UK.

Conflict of Interest

The authors declare no conflict of interest.

Author Contributions

Akshay Balachandran: Conceptualization (equal); Data curation (lead); Formal analysis (lead); Investigation (lead); Methodology (lead); Visualization (lead); Writing—original draft (lead); Writing—review & editing (lead). **Nair Abhigith Ravindran**: Visualization (supporting); Writing—review & editing (supporting). **Ghulam Mohd**: Investigation (supporting); Writing—review & editing (supporting). **Irfan Majeed Bhat**: Methodology (supporting); Writing—review & editing (supporting). **Saswati Priyadarshini**: Methodology (supporting); Writing—review & editing (supporting). **Saifullah Lone**: Conceptualization (lead); Data curation (equal); Funding acquisition (lead); Resources (lead); Supervision (lead); Validation (lead); Writing—review & editing (equal).

Data Availability Statement

The data that support the findings of this study are available from the corresponding author upon reasonable request.

Keywords

actuators, bioinspired, moisture, passive, sensitive, shrinkage

Received: July 18, 2024
Revised: September 12, 2024
Published online: October 29, 2024

[1] H. Hofhuis, A. Hay, *New Phytol.* **2017**, *216*, 339.
[2] C. Llorens, M. Argentina, N. Rojas, J. Westbrook, J. Dumais, X. Noblin, *J. R. Soc. Interface* **2016**, *13*, 20150930.
[3] J. N. Ma, B. Ma, Z. X. Wang, P. Song, D. D. Han, Y. L. Zhang, *Adv. Funct. Mater.* **2024**, *34*, 2308317.
[4] Y. Q. Liu, Z. D. Chen, D. D. Han, J. W. Mao, J. N. Ma, Y. L. Zhang, H. B. Sun, *Adv. Sci.* **2021**, *8*, 2002464.
[5] Y. L. Zhang, Y. Q. Liu, D. D. Han, J. N. Ma, D. Wang, X. B. Li, H. B. Sun, *Adv. Mater.* **2019**, *31*, 1901585.
[6] D. D. Han, Y. L. Zhang, H. B. Jiang, H. Xia, J. Feng, Q. D. Chen, H.-L. Xu, H. B. Sun, *Adv. Mater.* **2015**, *27*, 332.
[7] D. D. Han, Y. L. Zhang, Y. Liu, Y. Q. Liu, H. B. Jiang, B. Han, X.-Y. Fu, H. Ding, H.-L. Xu, H. B. Sun, *Adv. Funct. Mater.* **2015**, *25*, 4548.
[8] Y. Forterre, J. M. Skotheim, J. Dumais, L. Mahadevan, *Nature* **2005**, *433*, 421.
[9] A. Rafsanjani, V. Brulé, T. L. Western, D. Pasini, *Sci. Rep.* **2015**, *5*, 8064.
[10] M. Seale, A. Kiss, S. Bovio, I. Maria Viola, E. Mastropaolo, A. Boudaoud, N. Nakayama, *Nat. Commun.* **2022**, *13*, 2498.
[11] C. Dawson, J. F. V. Vincent, A. M. Rocca, *Nature* **1997**, *390*, 668.
[12] M. J. Harrington, K. Razghandi, F. Ditsch, L. Guiducci, M. Rueggeberg, J. W. C. Dunlop, P. Fratzl, C. Neinhuis, I. Burgert, *Nat. Commun.* **2011**, *2*, 337.
[13] R. Elbaum, L. Zaltzman, I. Burgert, P. Fratzl, *Science* **2007**, *316*, 884.
[14] Y. Abraham, C. Tamburu, E. Klein, *J. R. Soc. Interface* **2012**, *9*, 640.
[15] L. Jost, in *Lectures on Plant Physiology* (Ed: R. J. H. Gibson), vol. *3*, Clarendon Press, Oxford **1907**, pp. 405–417.
[16] E. P. Lacey, P. B. Kaufman, P. Dayanandan, *Bot. Gaz.* **1983**, *144*, 371.
[17] S. Armon, E. Efrati, R. Kupferman, E. Sharon, *Science* **2011**, *333*, 1726.
[18] J. Jiménez-Ruiz, L. Hardion, J. P. Del Monte, B. Vila, M. I. Santín-Montanyá, *Bot. Lett.* **2021**, *168*, 131.
[19] A. Balachandran, H. Parayilkalapurackal, S. Rajpoot, S. Lone, *ACS Appl. Bio Mater.* **2022**, *6*, 44.
[20] A. Danin, *Willdenowia* **2004**, *34*, 361.
[21] C. Ngernsaengsaruay, B. Puangsin, N. Leksungnoen, S. Khantayanuwong, P. Chanton, T. Thaepthup, P. Wessapak, R. Meeboonya, P. Yimlamai, K. Wanitpinyo, K. Chitbanyong, T. Andriyas, N. Banjatammanon, *Plants* **2023**, *12*, 1850.
[22] A. E. Al-Snafi, *Int. J. Phytopharm. Res.* **2015**, *6*, 34.
[23] R. Chaudhuri, S. Ghosal, *Phytochemistry* **1970**, *9*, 1895.
[24] L. Suárez, Z. Ortega, M. Barczewski, E. Cunningham, *Cellulose* **2023**, *30*, 4793.
[25] G. Easwaran, J. S. Packialakshmi, A. Syed, A. M. Elgorban, M. Vijayan, K. Sivakumar, K. Bhuvaneswari, G. Palanisamy, J. Lee, *Chemosphere* **2022**, *307*, 135951.
[26] H. Hachem, I. Mehrez, I. Boumnijel, A. Jemni, D. Mihoubi, *ACS Omega* **2023**, *8*, 12039.
[27] S. C. Nunes, A. P. Gomes, P. Nunes, M. Fernandes, A. Maia, E. Bacelar, J. Rocha, R. Cruz, A. Boatto, A. P. Ravishankar, S. Casal, S. Anand, V. de Zea Bermudez, A. L. Crespí, *Front. Plant Sci.* **2022**, *13*, 999252.
[28] M. Haworth, M. Centritto, A. Giovannelli, G. Marino, N. Proietti, D. Capitani, A. De Carlo, F. Loreto, *GCB Bioenergy* **2017**, *9*, 119.
[29] J. B. Gorce, I. J. Hewitt, D. Vella, *Langmuir* **2016**, *32*, 1560.
[30] G. Bamorovat Abadi, M. Bahrami, *Sci. Rep.* **2022**, *12*, 14867.
[31] J. Cai, E. Perfect, C. L. Cheng, H. Xu, *Langmuir* **2014**, *30*, 5142.
[32] M. N. Grigore, L. Ivanescu, C. Toma, *Halophytes: An Integrative Anatomical Study*, Springer, Switzerland **2014**.
[33] D. Gurera, B. Bhushan, *J. Colloid Interface Sci.* **2019**, *551*, 26.
[34] J. Ju, K. Xiao, X. Yao, H. Bai, L. Jiang, *Adv. Mater.* **2013**, *25*, 5937.
[35] D. Gurera, B. Bhushan, *Philos. Trans. R. Soc., A* **2019**, *377*.
[36] A. Balachandran, I. M. Bhat, G. Mohd, M. F. Wani, K. Majid, M. Wahid, S. Lone, *ACS Appl. Polym. Mater.* **2023**, *5*, 2272.
[37] G. Mohd, I. M. Bhat, I. Kakroo, A. Balachandran, R. Tabasum, K. Majid, M. F. Wani, U. Manna, G. Ghodake, S. Lone, *ACS Omega* **2024**, *9*, 12725.
[38] G. Mohd, K. Majid, S. Lone, *ACS Appl. Mater. Interfaces* **2022**, *14*, 4690.

© 2024 The Author(s). Advanced Intelligent Systems published by Wiley-VCH GmbH